Title
Approaches to Alter Particles Distribution in cryo-electron Microscopy Sample Preparation

Author
Zhou, Xueting

Publication Date
2020

Peer reviewed|Thesis/dissertation

UNIVERSITY OF CALIFORNIA

Los Angeles

Approaches to Alter Particles Distribution in cryo-electron Microscopy Sample Preparation

A thesis submitted for partial satisfaction of the requirements for the degree Master of Science in Microbiology, Immunology, and Molecular Genetics

by

Xueting Zhou

2020

ABSTRCT OF THE THESIS

Approaches to Alter Particles Distribution

in cryo-electron Microscopy Sample Preparation

by

Xueting Zhou

Master of Science in Microbiology, Immunology, and Molecular Genetics

University of California, Los Angeles, 2020

Professor Hong Zhou, Committee Chair

With the development of equipment and software, cryo electronic microscopy (cryoEM) was wildly used in structural biology to investigate biomolecular structure at atomic resolution. However, the sample quality is a barrier to pursuing higher resolution, including uneven distribution problems, heterogonous problems, and preferred orientation problems. Electron cryotomography (cryoET), a special application of cryoEM, have the advantage to resolve the 3D structure with a series of 2D tilting image at the same location, which is good to study the sample distribution in the thin ice layer. In this thesis, sample distribution was visualized by cryoET, and surfactant fluorinated fos choline 8 was used to manipulate the sample distribution. Besides, the principle underlying these problems were addressed based on calculation. Surface tension was the primary explanation for these problems.

The thesis of Xueting Zhou is approved.

Kent L Hill

Ting-Ting Wu

Hong Zhou, Committee Chair

University of California, Los Angeles

2020

Acknowledgements

I would like to thank my principal investigator and mentor, Dr. Z. Hong Zhou, for his continuous guidance and support. He led me into academic research since I was in undergraduate school. In the past two years, he inspired my passion for research, and show me that I can do more in the research field. With his guidance, I became a professional and rational researcher. He is the person that let me make the decision to apply to a Doctor degree for my next few years. I am truly fortunate to have him as my mentor.

Many Thanks to Dr. Ke Ding rose up this project and let me take over the project. When I worked with him, he shared his experience about the lab bench works with me. And I also want to thank Dr. Caiyan Wang, she helped me making progress on the project. My special thanks to Mr. Ivo Atanasov and Mr. Wong Hoi Hui who provide many technical supports. Many thanks to all lab mates who help me get through many difficult times.

In addition, a grateful thank you to Dr. Chun Xu, who was with me all the way from data collection to thesis writing. He demonstrated how to be a diligent and excellent researcher and spent plenty of time to guide me with his most patience. I appreciate your unconditional encouragement and support.

Last but not the least, I also want to thank my parents. They supported me all those years mentally and financially. They let me do whatever I want and stay on my side no matter what happens. I could not make it without them.

Table of Contents

Table of Figures

Table of Tables

Chapter 1 Introduction

1.1 Structural biology

Structural biology studies the molecular structure of biological macromolecules and investigates how alterations of those structures affect their function by explaining the biological phenomenon at a molecular level. Nowadays, with the development of science and technologies, the structure can be revealed using advanced technologies, and the scope of structures has reached the atomic level.

Three main methods are commonly used to study the molecular structures (Figure 1.1): X-ray crystallography, cryo electronic microscopy (cryoEM), and microcrystal electron diffraction (MicroED). X-ray crystallography is measuring the x-ray diffraction pattern after passing through a crystal, and it provides the information of 3D electron density of the crystal and the position of atoms. Comparing with X-ray crystallography, MicroED measures electron diffraction patterns to obtain structure information. In cryoEM, samples are embedded in vitreous ice. Electrons pass through the sample to form phase contrast between elastically scattered electrons and background electrons. The commons of these three methods are beams (X-rays or accelerated electrons) pass through molecules, and the distribution of the beams contained the information of the molecular structure. Since biomolecules are damaged by the beam radiation, averaging is used to get more actuate structure. Multiple molecules are used to collect data, and the structures are generated by averaging collected information on the nanocrystal of proteins. Among them, cryoEM shows unique advantages that it does not need a crystallization step, which avoids conformation changes.

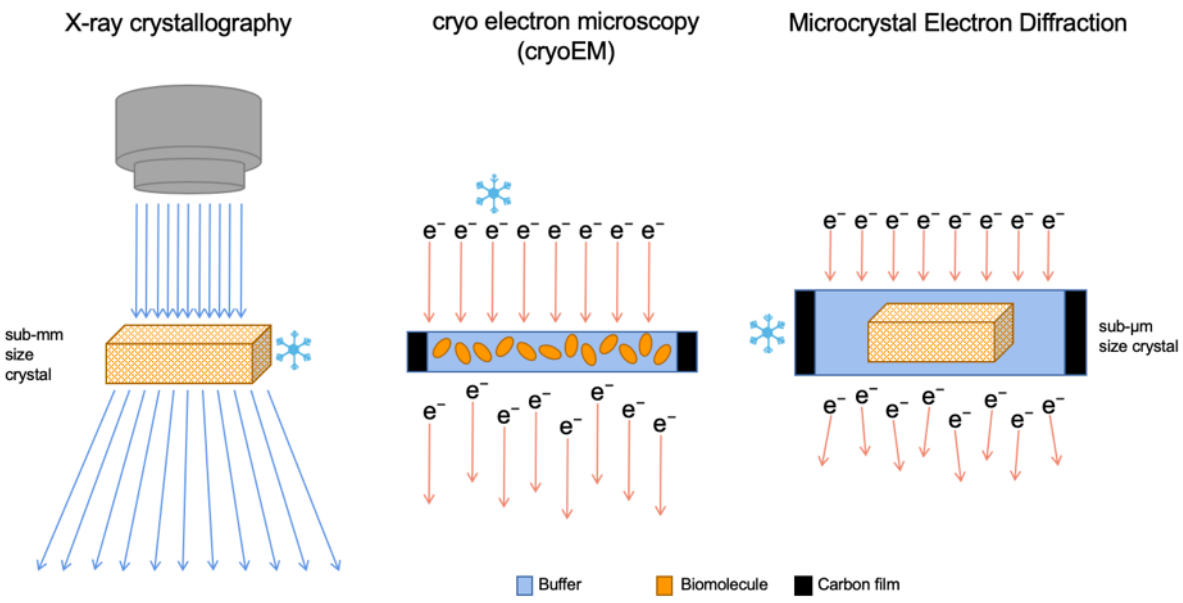

Figure 1.1 Three technologies for studying molecular stuctures. X-ray crystallography (left), cryoEM (middle) and Microcrystal Electron Diffraction (right).

1.2 cryoEM

In cryoEM, the sample was frozen in vitreous ice to protect biomolecules from radian damage [2] (Figure 1.2). The purified samples are applied to the carbon side and blotted by filter papers with setting temperature, humidity, blotting time, and blotting force to make the appropriated thickness of the ice. The ideal ice should be thick enough to cover the sample but not too thick, which leads to low contrast. The grid is plugged into the liquid ethane with high speed from vitreous ice instead of crystal ice. Vitreous ice can let electron beams pass with less diffraction. The grid is stored in liquid nitrogen for long-term use. After the grid is loaded to transmission electron microscopy (TEM), the gun emits electrons to pass through vitreous ice, and electrons form phase change due to the sample inside. The electron detector can collect the electron signals information and visualize it as bitmaps.

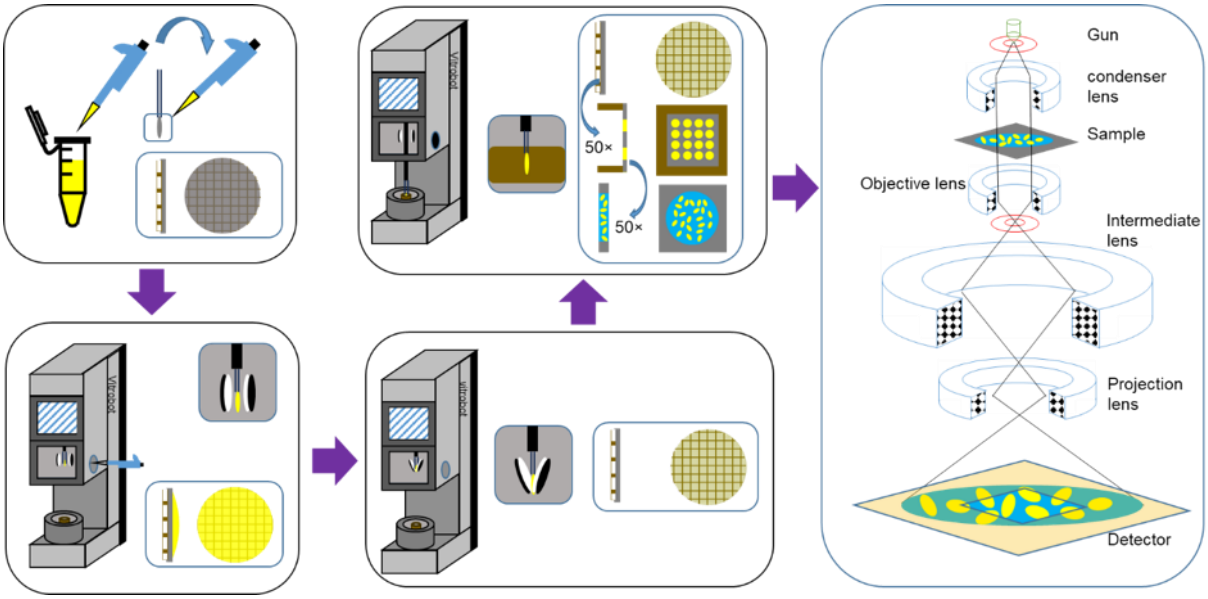

Figure 1.1 Workflow of sample preparation and imaging for cryoEM. Repudiation with permission of Ke Ding.

There are two conventional methods for cryoEM data processing: single particle analysis and electron cryotomography (cryoET). Single particle analysis is used to get near-atomic resolution reconstruction for viruses and protein [3]. At the same time, cryoET can reveal an in-situ 3D structure for biological macromolecules and cells with relatively low resolution [4].

In single particle analysis, many molecules can be averaged to reconstruct a reprehensive model and overcome the low signal to noise ratio problems. First, bitmaps are merged into a micrograph. If a movie with many frames is collected to peruse higher resolution, then the movie will be combined to a micrograph with frames' drift correction. Thousands of molecules in the micrographs are picked out from all micrographs. 2D averaging aligns the particles by searching the center of particles and in-plane rotation, which is used to evaluate the data quality. Then, the orientations of high-quality particles are determined by cross common line [5]and projection matching [6]. The particles' images are converted to 3D Fourier space by Fourier transform, and after reconstruction, invert Fourier transform are used to convert the 3D Fourier space to a 3D density map. More particles and more different orientations of the particle can contribute to a

higher resolution, which can demonstrate the side chains of proteins. The atomic protein models can build based on the density map to get the protein 3D structure.

CryoET is a particular application of cryoEM, which collects a series of 2D images with tilting the grids (Figure 1.3). Typically, the angles between grids and electron beams go from -60° to 60° with 1°or 2° increment. Since the ice thickness increases when the grids tilt to higher degrees, the electrons interact with larger ice areas leading to less information. Typically, the angle larger than -60° is not used in the data collection. The information in high angles is missing, causing "missing wedge" problems, which reduce the resolution [7]. To decrease the thickness of ice, large sample, like cells and tissues, might be prepared by cryo-sectioning [8] or focused ion beam (FIB) milling [9]. Since the tilt angle is determined for each image, series 2D images can be reconstructed to 3D tomogram for each tilting series by weighted back projections [10]or simultaneous iterative reconstruction technique (SIRT)[11]. Same as single particle analysis, averaging can increase the resolution by increasing signal to noise ratio. Subtomogram averaging is extract repeat unit as “particle” from the original tomogram and, then, align and average the particles to peruse higher resolution [12]. Comparing with single particle analysis, cryoET has less restriction for sample homogeneity and advantage of revealing in-situ structures.

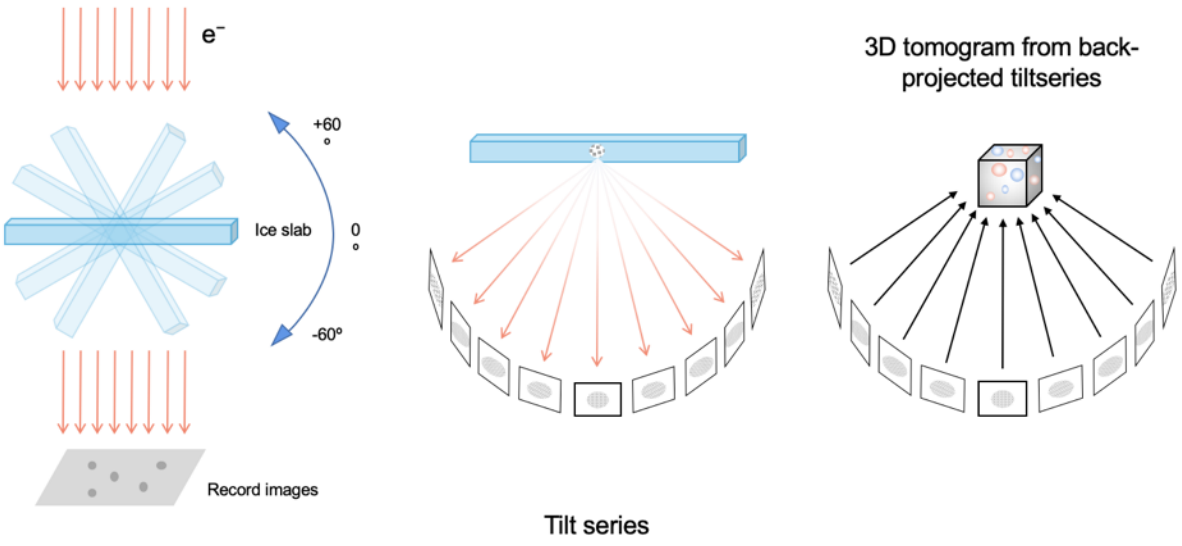

Figure 1.2 Schematic diagram of the concept and mechanism of cryoET.

1.3 cryoEM sample preparation

For cryoEM, a sample should be confirmed to be uniform before grid preparation. The negative stain is the typical examination to check the sample quality. For negative stain, the sample is applied to a carbon film grid and stained by heavy metal salt, like uranyl acetate. The extra stain is removed following by washing the grid. The background is stained while the samples are untouched, which make the morphology is visible. After a homologous negative stain image is acquired, the sample is ready to make cryoEM grids. However, the cryoEM result is not as good as the negative stain result and cannot move further for single particle analysis. The common problems include heterogeneous, unevenly distribution, and preferred orientation [13] (Figure 1.4). Like the crystallization in X-ray crystallography, the sample optimization is no universal method, and it is case by case. If the sample is not at its physiological state due to incorporated sample

preparation, the particle will not match with the existing projection in averaging.

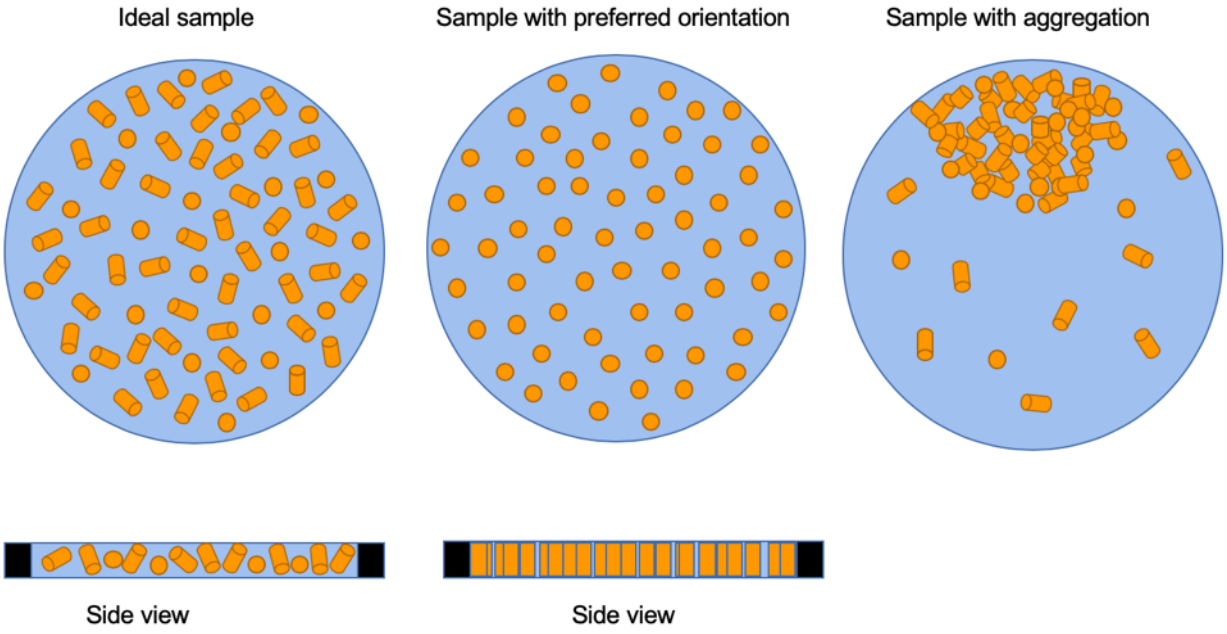

Figure 1.3 Schematic showing the sample distribution under different situations. Ideal sample(left), sample with preferred orientation problem(middle),and sample with aggration problems (right). Orange cyclindesrs represent biomolecules, blue background represents ice, and the black represents the edges of holes.

1.3.1 Air-water interface adsorption problem

CryoET can produce 3D tomogram from the reconstruction. Thus, it is an excellent method to reveal the 3D reconstruction of vitrified ice and sample in the hole on cryoEM grids. Each molecule can be labeled in the 3D tomograms to demonstrate the distribution of the molecules.

From the paper published by Alex J Nobel et al. [1] (Figure 1.5), the center thickness of ice ranges from 20 to 210nm with most around 100nm. In most cases, biomolecules are preferer to stay in the air-water interface area, with only one exception No. 19. The concentration of No.19 is extremely high that whole ice is fulfilled by sample densely. For other samples, we divided them into three categories: double adsorption, two-sided adsorption, and curved adsorption. For "double adsorption", the ice layer is so thin that only one layer of the sample can be embedded by ice. It is

hard to say which surface samples are close to. No. 6, 17, 21, 27, 34, 35, 38 are in this category. The second one is "two-sided adsorption". In this category, the ice thickness is much thicker than the diameter of the sample, so multiple lays of the sample is possible in this category. Besides, the ice is relatively flat. However, samples (No. 5, 7, 10, 12, 13, 14, 18, 22, 43, 46). are adsorbed to either one of the air-water interfaces or both air-water interfaces. In most cases, one air-water interface attracts more samples than the other side (No. 7, 10, 12, 13, 14, 43, 46). The last category is “curved adsorption”, which means at least one side of the ice is curved (No. 4, 33, 36, 39, 42, 44). The curve side normally adsorbed more molecules than the flat side (No. 33, 42, 44). From the observation, we can drive to the conclusion that molecules have air-water surface domain

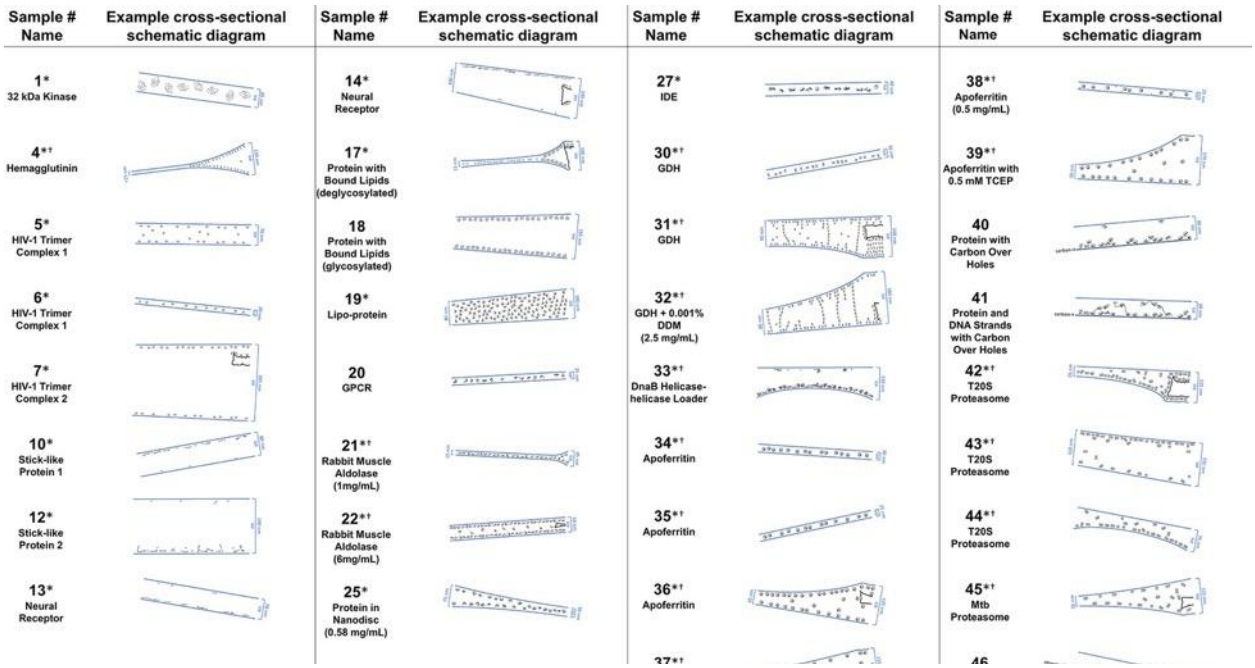

Figure 1.4 A selection of cross-sectional schematic diagrams of particle and ice behaviors in holes as depicted according to analysis of individual tomograms. The relative thicknesses of the ice in the cross-sections are depicted accurately. Each diagram is tilted corresponding to the tomogram from which it is derived; i.e. the depicted tilts represent the orientation of the objects in the field of view at zero-degree nominal stage tilt. If the sample concentration in solution is known, then it has been included below the sample name. Black lines on schematic edges are the grid film. The cross- sectional characteristics depicted here are not necessarily representative of the aggregate. Reproduced from ref [1].

problem than evenly distribute in the ice.

1.3.2 cryoEM sample heterogonous problem

Even though we try to control buffer pH, ionic strength, and many components to make the buffer close to the real environment in situ. However, the air-water interface is not a part of an in-situ environment, so that it might lead to sample physiological states changing in the preparation step. The structure we observe under cryoEM maybe not as the same as the sample physiological states.

Proteins stay in the air-water interface might lead to three kinds of physiological states change (Figure 1.6).

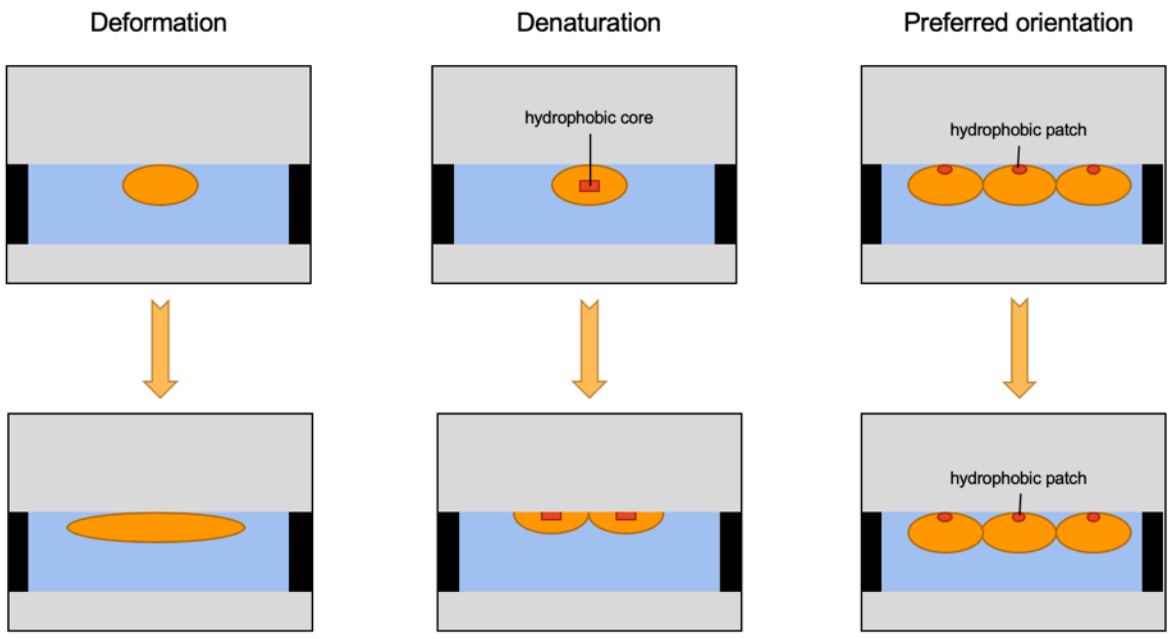

Figure 1.5 Three kinds of physiological states change due to air-water interface adsorption. Deformation (left), denaturation (middle), and preferred Orientation (right).

The first one is protein deformation [14], which means that protein conformation changes due to the outside force, in this case, is surface tension. The gradient of surface tension makes proteins

prefer to stable in a flatter conformation. Even though the pressure could be small, as long as the interaction is sufficiently long, the deformation will happen and be irreversible [15].

The second problem is protein denature. Protein structure contains four deferent levels, and hydrophobic core plays an essential role in protein folding [16]. The previous study shows [14, 17] that if the hydrophobic core is exposed, the protein is permanently denatured and cannot fold back again. Moreover, the air-water interface adsorption might unfold proteins and make them denatured. The protein denatured changes the conformation of the protein and induce the heterogeneity.

The third problem is preferred orientation. In single particle analysis, more orientations promise a better result in the data process. However, the hydrophobic patch protein surface or a flat surface prefer to stick to the air-water interface. If most particles are in similar orientation, it means the data of some directions are missing. Only the structure along the electron beam direction can be recorded. The 3D density map cannot present the structure exactly with incomplete 3D Fourier space information. Preferred orientation is a severe obstacle in numerous samples [2, 18-20].

Overall, the heterogeneity problem induced by protein deformation and denatured, and the preferred orientation problems will lead to problems in later data analysis and low resolution. The air-water interface is a potential reason to explain these phenomena. In this study, serval questions were illustrated, including different sample behaviors between negative stain and cryoEM, the influence of the sample concentration influence particle distribution, and the potential of manipulating particle distribution using a surfactant. The high-quality sample is fundamental for later data processing and high resolution. cryoET data presents the 3D particle destruction in ice, providing experimental evidence. Theoretical calculation explained the principle underlying the phenomenon.

Chapter 2 Materials and Methods

2.1 Protein preparation and storage

Chaperonin 60 lyophilized powder (GroEL, 1 mg) from *Escherichia coli* (Cat # C7688, Sigma-Aldrich, St. Louis, MO, USA) was solubilized in 0.2 mL Tris buffer (50 mM, pH 7.5, containing 10 mM KCl and 10 mM $MgCl_2$). NanoDrop Microvolume Spectrophotometers and Fluorometer measured the concentration of the GroEL. GroEL stock solutions were prepared by diluting the above solution with the same buffer to 2 mg/mL, and aliquoting into 10 Eppendorf tubes (20 µL each). The GroEL stock solutions were stored at -80 °C for long term storage and thaw before use. Defrosted GroEL solutions were stored at 4 °C and used within 2 weeks.

2.2 Sample preparation for negative staining

For negative staining, GroEL stock solutions were made dilutions in 1 mg/mL, 0.1mg/mL, and 0.01 mg/mL using GroEL buffer. The transmission electron microscopy grids were 400 mesh Cu grids with support films of Formvar and Carbon Type-B (prod # 01814-F, TED PELLA INC, Redding, CA, USA). Grids were glow discharged by PELCO easiGlow for 30 seconds. 2.5 µL GroEL solution was applied to the TEM grid. After 1 minute, the extra sample was removed by blot paper. Then 5.0 µL uranyl acetate (2 %) was applied to the grid and repeated the similar removing process after 1 minute. Additional 5.0 µL uranyl acetate was applied again and blotted immediately. Grids were air-dried in room temperature.

2.3 Sample preparation for cryoET

GroEL stock solutions were diluted to 0.4 and 1 mg/mL with the Tris buffer. GroEL sample in each concentration was equally separated into 2 groups, one with the surfactant, while the other one with buffer (Table 2.1). For the surfactant group, 0.03 and 0.3 mg/mL fluorinated fos-choline

8 were added to both 0.4 and 1 mg/mL GroEL solutions. The volume difference for each sample was fulfilled up with the buffer. After that, the samples were mixed with 1:70 diluted 5-nm diameter fiducial gold beads in a 10:1 volume ratio for non-surfactant sample, and in 8:1 for GroEL samples with surfactant with additional buffer to fulfill the volume gap. FEI Vitrobot Mark IV was used to make a vitrified sample. An aliquot of 2.5 µl of the sample was applied to 200 mesh Cu Quantifoil 100 holey carbon films (R 2/1), which were glow discharged by PELCO easiGlow for 30 seconds. The grids were blotted by filter papers from both sides under 10 °C and 100 % humidity for 10s with a force of 10, except for sample with 3 mM fluorinated fos-choline 8 concentration, which used 6.5s, and immediately plunged into solid-liquid coexisting ethane. Grids were transferred to liquid nitrogen and stored.

Table 2.1 Summary of sample preperation and data collection

GroEL concentration	0.4mg/mL	1.0mg/mL				2.0mg/mL			
fluorinated fos-choline 8 concentration	0	3mM	0.3mM	0.03mM	NA	3mM	0.3mM	0.03mM	NA
Numbers of tomogram collection	3	0	3	3	3	0	3	3	3

2.4 Imaging with electron microscopy

Transmission electron microscopy imaging was performed on the FEI Tecnai TF20 at 200 kV equipped with a TIETZ F415MP 16-megapixel CCD camera. The pixel size was 0.4433 nm at x50,000 magnification**.** Negative stain images were collected at x50,000 magnification**.** Cryo samples were imaged using the low-dose mode to optimize the plunge-freezing conditions before cryo Tomography data collection. Images were searched at x5,000 magnification and collected at

x50,000 magnification. FEI TEM Batch Tomography was used to collect the cryoET tilt series bi-directionally from -50° to +50° with 2° increments. TEM Imaging & Analysis (TIA) was used to acquire data. Tilt series were collected with 15,000~25,000 counts/nm^2/s. Exposure time was adjusted to distribute in the whole series with a 1.4 intensity ratio ($I_{0°}$/ $I_{60°}$). The cumulative dose count was 50~60 $e^-/Å^2$ per tilt series. Data was collected on CCD camera under Exposure mode with binning 2 (bottom-right pixel 2048 x 2048). Search mode was used to find the locations at x5,000 magnification to collect tilt series, focus mode was used to track the images at x50,000 magnification during data collection, and exposure mode was used to collect tilt series at x50,000 magnifications. Filter that cut off long wavelength at 50 nm (Radius), 5n m (Sigma), and cut off short wavelength at 10nm (Radius), 5nm (Sigma) was applied to get a good cross-correlation. The defocus value set at -6 µm. Each tilt series was collected in about 25 minutes. The amount of tilt series for each condition was shown in the following tables.

2.5 Data processing

The tilt series were reconstructed by Etomo component of the IMOD software package [10] to 3D tomograms. "Build Tomogram" was chosen to start the reconstruction process. Tilt series images were pre-processed by removing the outlier pixel values in the data files. Coarsely alignment was done before fine alignment using the fiducial seeding model. 10 to 15 gold beads were picked for each tilt series, and the specimen-movements mathematical model was used to predict gold beads positions. The mean residual error was reduced during fine alignment by fixed big residual. Positioning tomogram thickness was set to 1000 to include the top and bottom air-water interface. The tilt axis and Z shift were also computed and adjusted to create final alignment. The final tomograms were build using SIRT with 10 iterations. Finally, the whole tomogram was rotated around the x-axis to make the air-water interface roughly parallel with the field of view.

To locate GroEL, all proteins were selected in IMOD and saved as a mod file. The coordinates of the particle were recorded and can be visualized in a 3D model by IMOD. All proteins were classified based on different orientations.

Since the ice contaminations were attached after vitreous ice formed, they were on the air-water interface. The ice contaminations were used as a marker to locate the air-water interface. The last tomogram slice contained the ice contamination was the closest plane to the air-water interface, and it was recognized as the air-water interface. Two air-water interfaces were located used the same way, and the distance between two interfaces was ice thickness. Some tomograms also include the edge of the hole to help identify the air-water interface. The reconstructed tomogram was rotated 90° via x-axis in IMOD to observe the side view of the grids, and the image thickness set to 20. Some air-water interfaces can barely be visualized. The estimated error between the real ice thickness and the distance measured from the ice contamination layers is several nanometers.

Chapter 3 Results

3.1 Protein adsorbed on the surface by single particle EM

In X-ray reflection experiments [21] [14] and spectroscopy [22], people observed the phenomena that proteins are adsorbed to the surface. The same phenomena also happen in electron microscopy results.

The actual protein number in cryoEM is compared with the theoretical protein number to quantify surface adsorption. The actual protein number in each view of published single particle images are counted. The theoretical protein number is calculated based on the bulk volume concentration and molecular weight of the sample. Three proteins are analyzed: GroEL [23]

(800kDa), β-galactosidase [24] (465kDa) and hemoglobin [25] (64kDa). The ice is assumed to be flat with 50nm thickness. The actual to theoretical ratio is calculated (table 2.1). The actual to theoretical ratios three proteins are more than 10, which means the more proteins we can see in each micrograph than the protein in bulk volume. The reason behind this phenomenon is surface adsorption. In the thin buffer layer, the surface to volume ratio is high, and surface adsorption increases the amount of particle dramatically. GroEL has severe surface adsorption problems because of the highest actual to theoretical ratio. Besides, GroEL belongs to the chaperonin family, and the structure is stable and known [26] [23], which makes it a perfect test object for later experiments.

Table 3.1 Quantify the surface adsorption by calculating numbers of particles in one view.

	GroEL	β-galactosidase	haemoglobin
Concentration (mg/mL)	0.1	2.3	1.5
Molecular weight (kDa)	800	465	64
View volume (mL)	9.43E-16	2.75E-15	4.18E-15
Theoretical Number in the view	0.73	8.19	21.13
Actual number in the view	99	110	240
Actual/Theoretical	135.62	13.43	11.36

3.2 Protein distribution in samples with or without surfactant

3.2.1 Negative stain result

A negative stain result was used to confirm the sample homogeneity. GroEL in different concentrations with negative stain was imaged under electronic transmission microscopy. 1.0mg/mL, 0.1mg/mL, and 0.01mg/mL GroEL were done for negative stain, and 0.01mg/mL is the best concentration because the particles distribute evenly in one layer without overlapping

(Figure 3.1). The particle presents homogeneity and strong preferred orientation. Majority particles are top view in the figure.

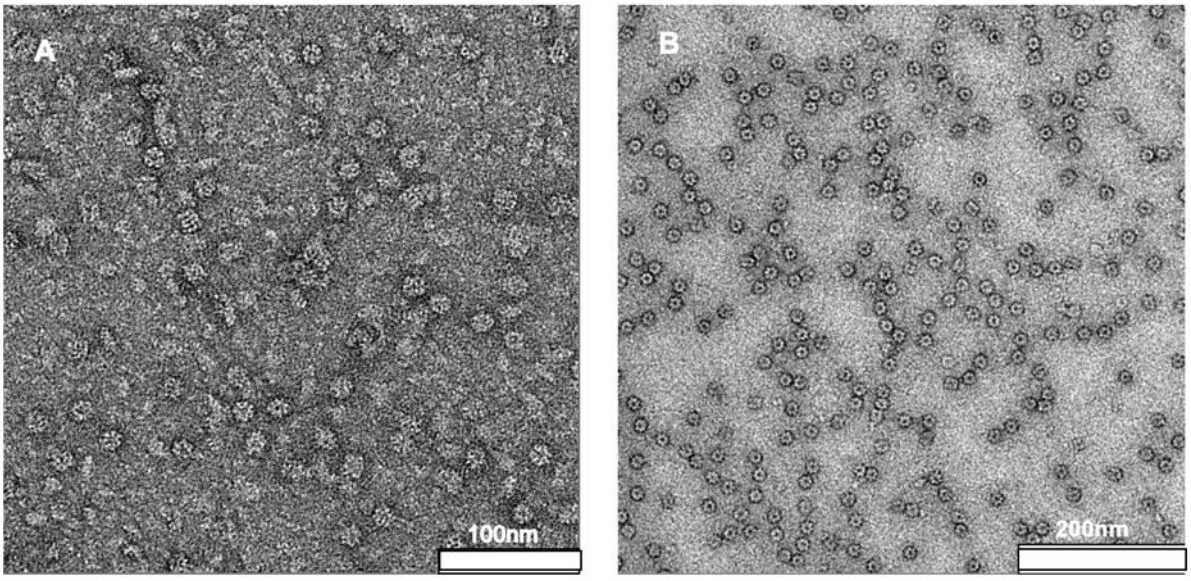

Figure 3.1 TEM images of GroEL after negative staining. The concentration of GroEL is 0.1mg/mL (A) and 0.01mg/mL(B).

3.2.2 Ice thickness

CryoET collects multiple images at the same position with different orientation and reconstructs to a 3D structure. It presents the 3D structure in the ice and visualizes the position for each particle. In all tomograms, flat ice is produced. The ice thickness was measured by ice contamination as it described the method part, and it ranges from 45 to 80 nm (Table 3.2). The ice thickness might be affected by many parameters, including but not limited to sample concentration, blotting force, blotting time, and different areas on grids. GroEL is 145 Å height and 135 Å in diameter [27], and the ice is thick enough to hold multiple layers of GroEL.

Table 2.2 Summary of ice thickness for GroEL in different concentration

	0.4 mg/mL GroEL	1.0 mg/mL GroEL	2.0 mg/mL GroEL
Tomogram 1	57 nm	80 nm	62 nm
Tomogram 2	45 nm	60 nm	67 nm
Tomogram 3	53 nm	66 nm	63 nm

3.2.3 Influence of sample concentrations

Tomograms for GroEL in concentration 0.4 mg/mL, 1.0 mg/mL, and 2 mg/mL on Cu Quantifoil grids. All proteins in each tomogram were boxed, and the coordination was recorded to study the distribution and orientation (Table 3.3). The proteins whose center were within 10 nm from the air-water interface were defined as being on the air-water interface. For GroEL, there were two dominant orientations, and the average preferred orientation ratio was 90 % on top view, and 10 % on the side view. The other orientations cannot be identified. 3D classification needs to be done to classify orientations, which is more accurate.

Table 3.3 Summary of distribution and orientation of particles with no surfactant

	0.4mg/mL GroEL	1.0mg/mL GroEL	2.0mg/mL GroEL
Total number of particles	119	296	793
Number of particles on the blotting surface (percentage)	119 (100%)	296 (100%)	683 (86.1%)
Number of particles on the non-blotting surface (percentage)	0 (0%)	0 (0%)	88 (13.9%)
Amount of protein in bulk (percentage)	0 (0%)	0 (0%)	0 (0%)
Amount of protein on top view (percentage)	111 (93.3%)	270 (91.2%)	683 (86.1%)

Amount of protein on side view (percentage)	8 (6.7%)	26 (8.8%)	110 (13.9%)
Amount of protein on other view (percentage)	0 (0%)	0 (0%)	0 (0%)

From the top view of the tomogram, only for 2.0 mg/mL GroEL occupied the air-water interface entirely (Figure 3.2). The cross-section of picking particles model shows particle distribution, with the tilting angle of the tomogram related to the electron beam. Only in 2.0 mg/mL GroEL sample, proteins diffuse to the other side with no protein in bulk. Since the air-water interface is not obviously visible in tomograms, schematic diagrams of crossing-section of ice for representative tomograms. Ice thickness and particle sizes are approximate to scale, and the number of the particles is approximate, not an exact number.

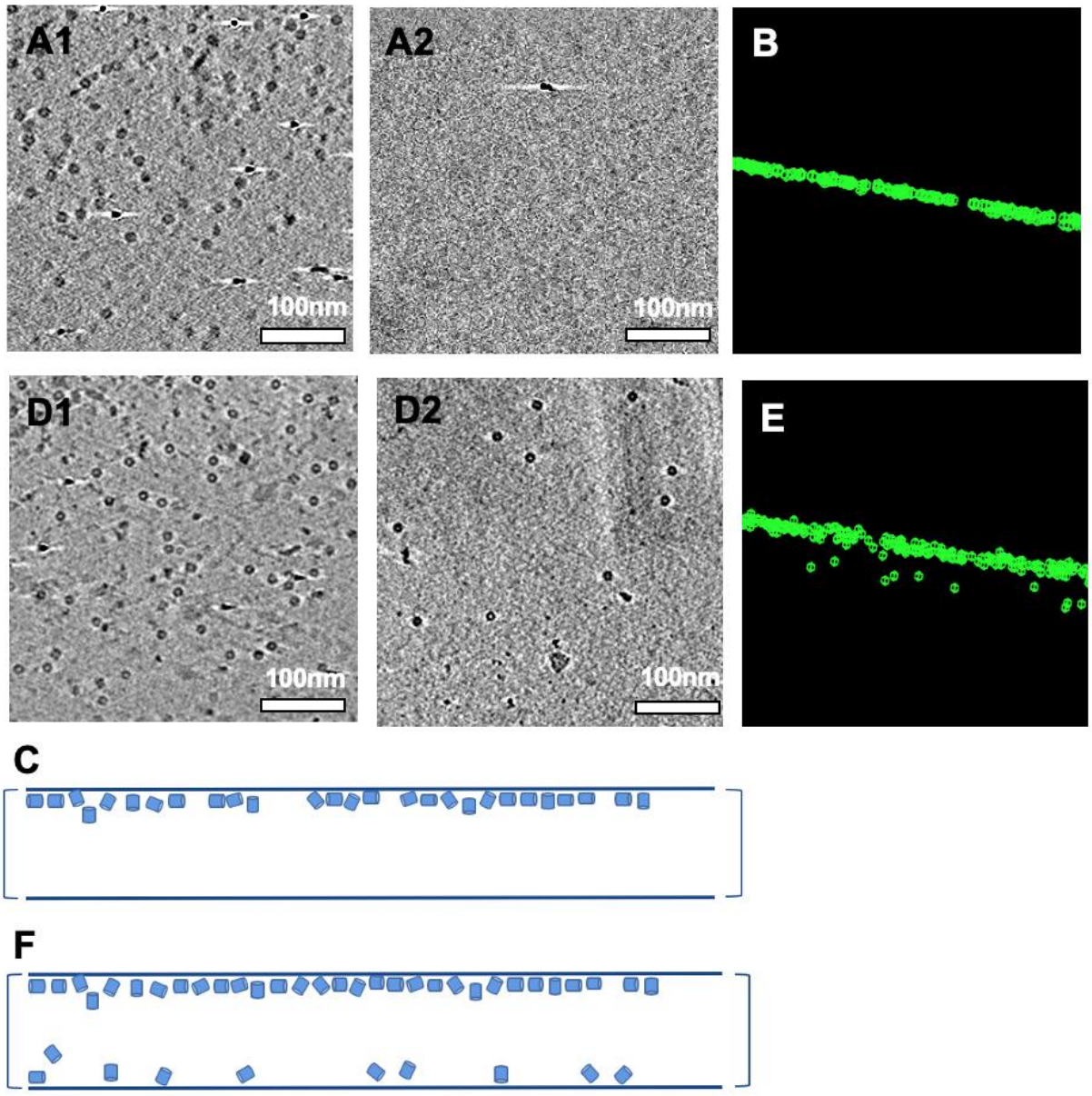

Figure 3.2 CryoEM and particle model and schematic model of cross-section for GroEL sample. A, B, and C is for 1mg/mL GroEL. D, E, F is for 2mg/mL. A1, A2 and D1, D2 are cryoEM images of the two air-water interfaces.

3.3.4 Application of surfactant

The surfactant can decrease the surface tension on the air-water interface and relieve the surface adsorption-related issues [19] [28]. The hydrophobic head of the surfactant stick on the air-water interface and hydrophilic tail in the water make it decrease the surface energy. The surfactant occupies the air-water interface. Meanwhile, the surface absorbance contributes to the amount of protein we see in one view; the application of surfactant decreases the number of proteins (figure 3.3).

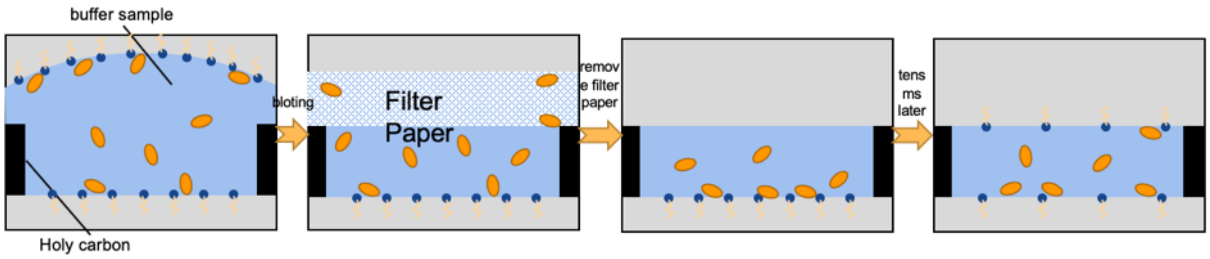

Figure 3.3 Surfactant change the sample distribution by decrease the surface tension.

When we do biomolecular research, many types of surfactants are used for different purposes. Inducing surfactant into the buffer is not only can decrease the surface tension but also lead to protein's physiological state changing with high concentration (Figure 3.5), especially for ionic surfactant. Appropriated types of surfactant and concertation should be chosen for alternating cryoEM sample distribution. A weaker surfactant may not block proteins from the air-water interface by weak surface pressure [29]. Besides, micelles with a similar size, the protein sample will reduce the signal to noise ratio (Figure 3.4). The best candidates might be various case by case.

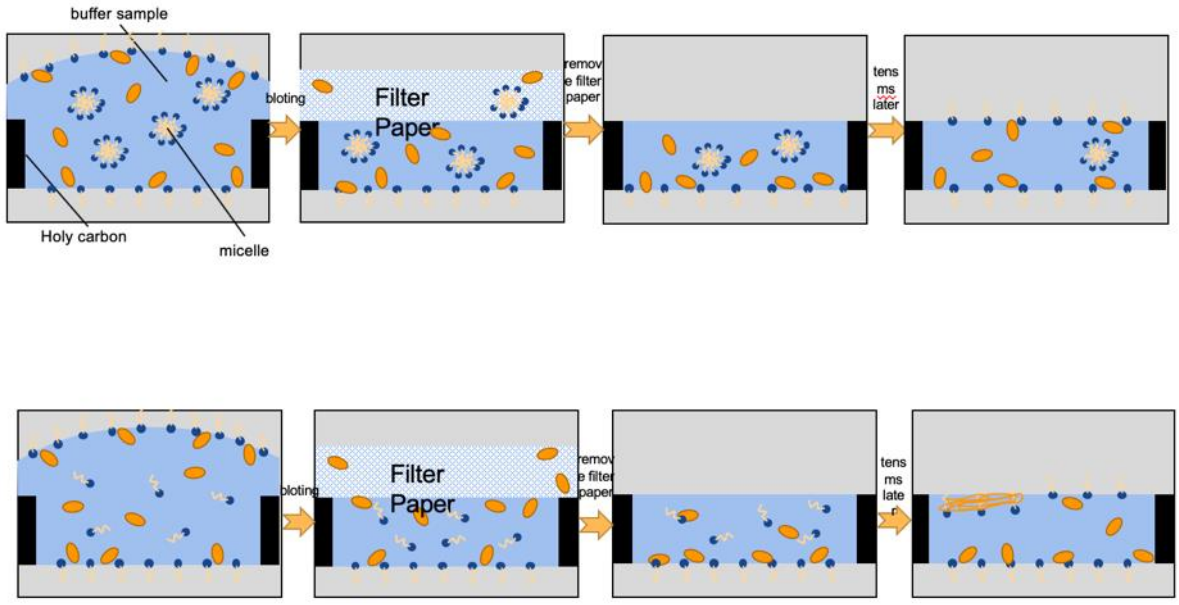

Figure 3.4 Surfactant can induce problem for cryoEM sample. Surfactant makes protein structure denatured(top), and surfactant forms micelle increasing the background noise(bottom).

Fluorinated surfactants are commonly used in cryoEM sample preparation. The previous study demonstrates that fluorinated surfactants contribute to a thin layer of buffer and vitrification [29-32](Figure 3.6). The critical micelle concentration (CMC) of fluorinated fos-choline 8 is 2.9mM, and it is relatively high compare with the CMC for many surfactants, which are less than 1mM. The high CMC value can avoid micelles problems with a broad range of possible concentrations. Besides, the surface pressure of fluorinated surfactants is higher than hydrocarbon surfactants [33] and has an advantage in blocking protein from the air-water interface. A tail that is both hydrophobic and oleophobic can make surfactants milder. Fluorinated surfactants have this kind of tail and make them have a low possibility to denature biomolecules [34]. Overall, fluorinated fos-choline 8 is a perfect candidate for manipulating biomolecules distribution in cryoEM.

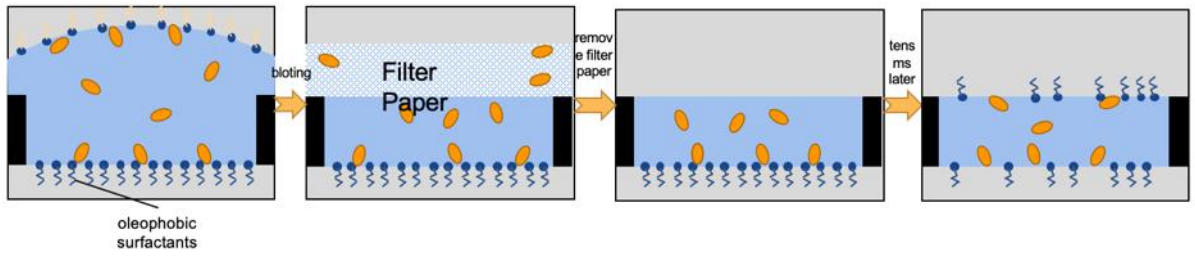

Figure 3.5 Theoretically, fluorinated fos-choline 8 can manipulate biomolecules distribution effectively without introducing other problems.

To find a suitable concentration for fluorinated fos-choline 8, 3.00, 0.30 and 0.03 mM fluorinated fos-choline 8 were add to GroEL with either 1.0 or 2.0 mg/mL.

It is noted that the ice thickness of the sample with a surfactant are alternated. With 1.00 mM fluorinated fos-choline 8, a thin ice layer cannot form under the same blotting parameters (blotting time: 10S, blotting force 10). To make sure the ice thickness for 3.00 mM fluorinated fos-choline 8 falls into the same range with the buffer without fluorinated fos-choline 8, the blotting time was alternated to 6.5s. For relatively low fluorinated fos-choline 8 concertation (0.3 and 0.03 mM, respectively), the blotting parameter can be the same set with no surfactant group to form good thin vitreous ice.

3mM fluorinated fos-choline 8 induced severe aggregation problems into the sample (Figure 3.7A). Most proteins were not in their physiological states. With 0.3mM fluorinated fos-choline 8, some proteins were aggregate while the rest of them were under acceptable conditions (Figure 3.7 B). With 0.03mM fluorinated fos-choline 8, there is no obvious aggregation problem (Figure 3.7 C). Besides, comparing with the sample without surfactant (Figure 3.7D), the surfactant made the number of particles in the same area deceasing.

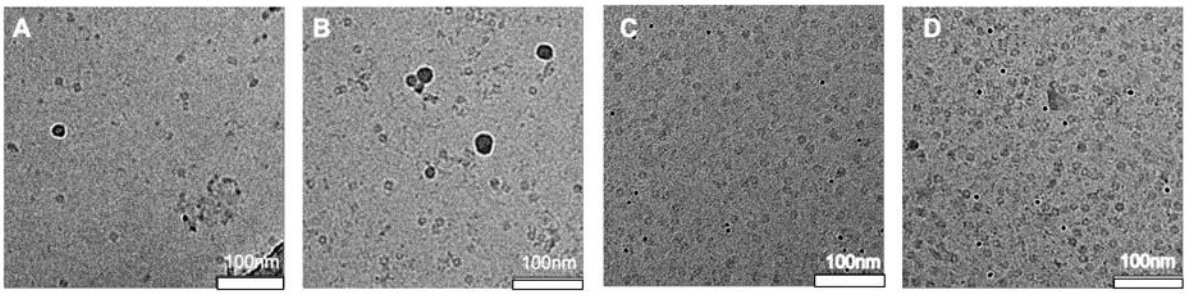

Figure 3.6 CryoEM images of 2 mg/mL GroEL with different concentrations of fluorinated fos-choline 8. From right to left, the concentration of fluorinated fos-choline 8 is 3mM(A), 0.3mM(B), 0.03mM(C), and 0mM(D), respectively.

The tomograms were taken for 0.3mM and 0.03mM fluorinated fos-choline 8, and particles were boxed (Table 3.4). The area of a hole on a grid was different for each tomogram.

Table 3.4 Summary of distribution and orientation of particles with fluorinated fos-choline 8.

	1.0 mg/mL GroEL			2.0 mg/mL GroEL		
Concentration of fluorinated fos-choline	0.3mM	0.03mM	0mM	0.3mM	0.03mM	0mM
Total number of particles	296	213	296	509	852	793
Number of particles on the non-blotting surface (percentage)	169 (57.1%)	127 (59.6%)	296 (100%)	260 (51.1%)	426 (50.0%)	683 (86.1%)
Number of particles on the blotting surface (percentage)	60 (20.2%)	41 (19.2%)	0 (0%)	116 (22.8%)	210 (24.6%)	88 (13.9%)
Amount of protein in bulk (percentage)	67 (22.6%)	45 (21.1%)	0 (0%)	133 (26.1%)	216 (25.4%)	0 (0%)

Amount of protein on top view (percentage)	260 (87.8%)	192 (90.1%)	270 (91.2%)	443 (87.0%)	724 (85.0%)	683 (86.1%)
Amount of protein on side view (percentage)	36 (12.2%)	27 (9.9%)	26 (8.8%)	66 (13.0%)	128 (15.0%)	110 (13.9%)
Amount of protein on other view (percentage)	0 (0%)	0 (0%)	0 (0%)	0 (0%)	0 (0%)	0 (0%)

With no fluorinated fos-choline 8, all proteins were on the non-blotting side for 1mg/mL GroEL, and 86.1% of proteins were on the non-blotting side for 2mg/mL GroEL. After adding 0.03mM fluorinated fos-choline 8 to 1mg/mL GroEL, protein distribution was rearranged.19.2% of proteins were in bulk, and 21.1% of proteins were on the blotting surface. With 0.3mM fluorinated fos-choline 8 in 1mg/mL GroEL, 03mM fluorinated fos-choline 8 located in bulk, and 22.6% of proteins were on the blotting surface. For 2mg/mL GroEL, which had protein on two surfaces without any surfactant, fluorinated fos-choline 8 increased protein in bulk by 25.4% for 0.03mM, and 26.1% for 0.3mM (Figure 3.8). The protein orientation ratio did not have significant change with fluorinated fos-choline 8.

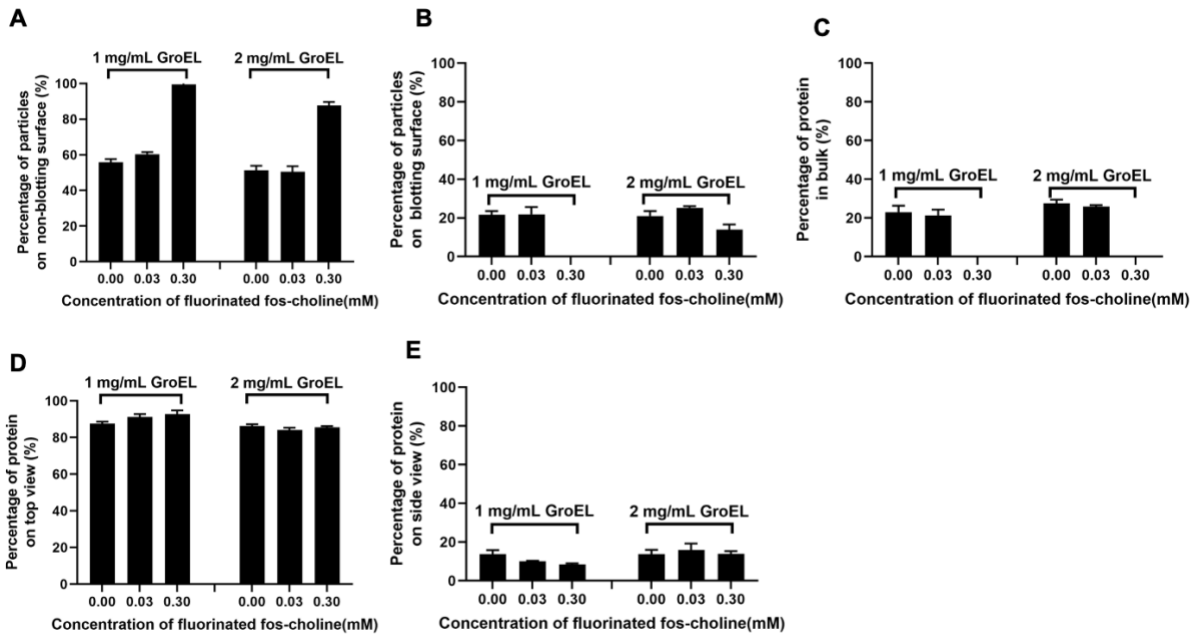

Figure 3.7 Histogram of percentage of protein in different positions and orientations. The error bars are mean +/- standard deviation with N=3.

It shows that particle distribution was significantly alternated the distribution by pushing proteins adsorbed on the surface to bulk. From tomogram results, proteins appeared on different slides indicating that they are on different positions in ice (Figure 3.9). The crossing-section of the particle model provides consistent information. However, the preferred orientation problem was not solved because the orientation ratio did not have obviously changing. If the 3D classification is done, more information about orientation can be provided.

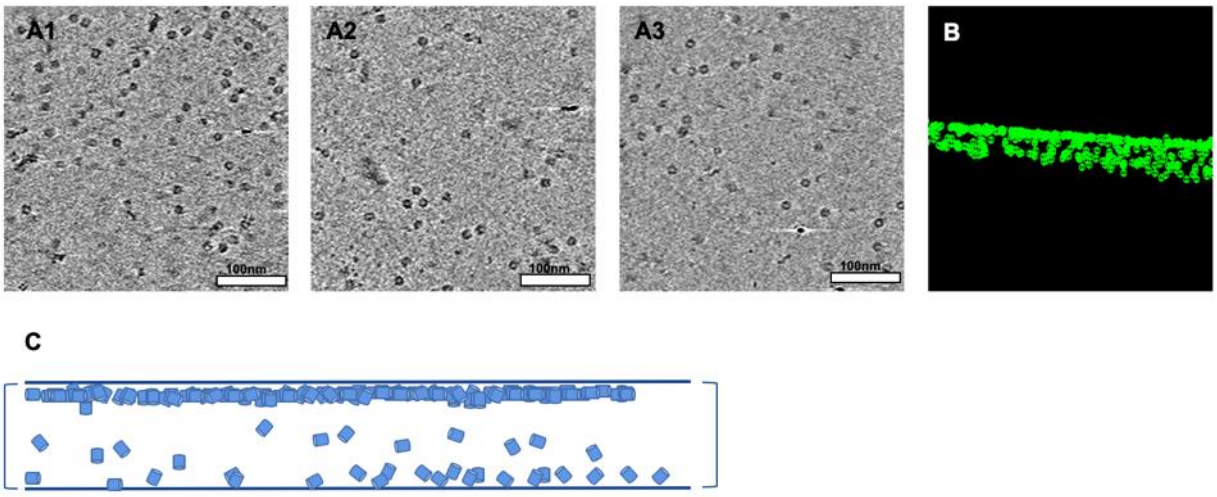

Figure 3.8 cryoEM and particle model and schematic model of cross-section for 2mg/mL GroEL with 0.03mM fluorinated fos-choline 8. A1 is the cryoEM image for non-blotting surface, A2 is the cryoEM image for bulk volume, and A3 is the cryoEM image for blotting surface. B is the particle model of cross-section. C is the schematic model of cross section.

Chapter 4 Discussion

The experiment result shows that a high concentration of fluorinated fos-choline 8 can induce protein denaturation and aggregation problems. 0.3mM and 0.03mM fluorinated fos-choline 8 has a similar influence on sample distribution, while 0.3mM fluorinated fos-choline 8 has a risk of protein denaturation.

To explain the reason behind sample heterogonous and distribution phenomenon, we need to scope down to the molecular level to see the intermolecular force between proteins and buffer, and proteins.

4.1 Air-Water Interface Interaction with Samples

When the electron beam passes through the ice, elastically scattered electrons and background electrons create phase contrast to produce the cryoEM Images. Meanwhile, the inelastically

scattered electrons produce noise and will decrease the contrast. The thicker ice will lead to more inelastically scattered electrons because electrons will travel longer distances in the ice. Since the buffer density and proteins density are close, phase contrast in cryoEM image is low. Thus, having a thin buffer layer is vital in sample preparation. Usually, cryo TEM samples are not thicker than 500nm [35]. For the cryoEM sample, most of sample ice thickness is between 10nm to 200nm.

CryoEM samples should be fully covered by ice to protect the sample from electron radiation. Currently, the smallest protein cryoEM can resolve is 50kDa [36]. Based on protein average density of 1.37 g/cm3, the protein diameter is 4.9nm. Nucleocytoplasmic giant DNA viruses [37] with 190nm diameter is the most massive structure currently solved by cryoEM with atomic resolution. The sample size range (5 nm – 190 nm) falls into the cryoEM ideal ice thickness range (10 nm - 200 nm).

In buffer, the interaction between biomolecules, and molecular with the air-water interface are the primary force on biomolecules. Proteins have charges on their surface in the buffer, so the Debye-Hückel length was used to calculate what distance two proteins can be recognized as electric neutrality. The Debye-Hückel length is defined by

$$\lambda_D = \left(\frac{\epsilon k_B T}{\sum_{j=1}^{N} n_j^0 q_j^2} \right)^{1/2}$$

where ϵ is the relative static permittivity of solvent, k_B is Boltzmann's constant, T is the temperature, n_j is the mean concentration of charges of the species j, and q_j is the charge of the species j. The Debye length is 0.7nm [38] in 1X Phosphate Buffered Saline (PBS) at room temperature, which is similar to the environment in the cell. It is smaller than the protein secondary

structure alpha-helixes, whose diameter is 1.2nm. It means two proteins have to be extremely close to making two biomolecules in bulk have effective interaction.

Knudsen layer thickness is used to describe the local region that gas interacts with liquid/solid at their interface, which is a perfect parameter to quantify the air-water interface. Knudsen layer thickness is close to l_c , mean free path, of air. l_c is defined by

$$l_c = \frac{k_B T_s}{\pi d^2 p_s}$$

where k_B is Boltzmann's constant, T_s is room temperature, p_s is atmosphere pressure, and d is the molecular diameter. 68nm is the mean free path of air [39] [40], which means air can work on the buffer within 68nm from the air-water interface into the buffer at room temperature and atmospheric pressure. It is also much longer than Debye-Hückel's length, and it proves that the air-water interface affects biomolecules dominantly. The calculation illuminates that the air-water interface is the essential reason for sample heterogonous problem.

4.2 Explanation of sample distribution

In the whole system, the total energy always tends to remain at a low level. To explain why staying on the surface is the favorable state for biomolecules, the energy for the ice system is calculated (Figure 4.1).

Surface energy is the extra energy generated during a new surface is produced. The overall surface energy when a biomolecule in bulk volume is defined by

$$E_{bulk} = 2A_1\gamma_{lg} + 2A_2\gamma_{ls}$$

where A_1 is the surface area of the one hole on a grid, $A_2$is the one side of surface area that molecule interacts with liquid or air, γ_{lg} is surface energy on liquid-gas surface, and γ_{ls} is surface energy on the liquid-solid surface.

If the sample can adsorb on one air-water interface, the overall surface energy is defined by

$$E_{single\_adsorption} = 2A_1\gamma_{lg} + A_2\gamma_{ls} + A_2\gamma_{sg} - A_2\gamma_{lg}$$

where and A_1, A_2, γ_{lg}, γ_{ls} are the same as before, and γ_{sg} is surface energy on the solid-gas surface. To Compare the surface energy between E_{bulk} and $E_{single\_adsorption}$,

$$E_{single\_adsorption} - E_{bulk} = A_2\gamma_{sg} - A_2\gamma_{lg} - A_2\gamma_{ls}$$

the overall surface energy is decreasing in $E_{single\_adsorption}$ because the γ_{lg} (surface tension) for water is large (72mN/m). As long as the water-air interface area is decreasing, the overall surface for the ice system is decreasing, and it makes the whole system more stable and favorable than the partials in bulk.

If the buffer layer goes thinner, the particle will be double adsorption. The total surface energy will further decrease, and the difference

$$E_{double\_adsorption} - E_{single\_adsorption} = A_2\gamma_{sg} - A_2\gamma_{lg} - A_2\gamma_{ls}$$

is usually less than 0 for the same reason. Based on the calculation, double adsorption is the most energetically favored status. Moreover, it will happen in a thin buffer layer.

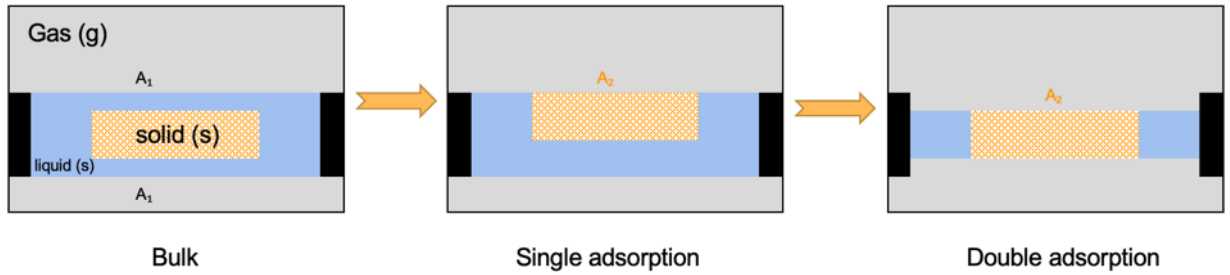

Figure 4.1 Schematic diagram of surface energy for different sample position.

In the blotting step, the extra buffer with particles is removed by filter paper, usually from one side. The ice shape depends on how much buffer left after blotting. If there is a little buffer left, the surface is concave. Otherwise, the surface is flat (Figure 4.2).

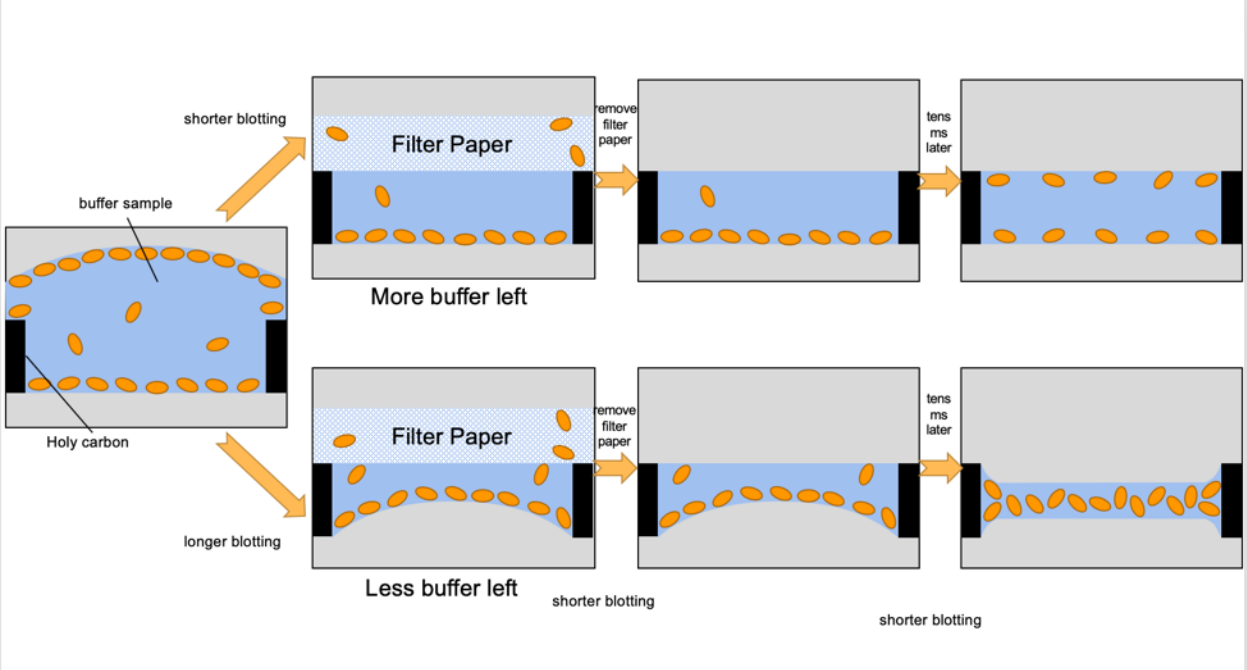

Figure 4.2 Ice shape and protein distribution based on amount of remain buffer. Flat ice with more remaining buffer (top) and concave ice with less remaining buffer.

Biomolecules on the blotting side are removed by filter paper. The particle concertation affects the sample distribution. If the non-blotting side surface is not fully occupied, all particles have already stayed in energetically favored status. If the non-blotting side surface is fully occupied and some

particles are remaining in bulk, the particles in bulk will diffuse to the new empty surface to decrease the total surface energy in the ice system. The sample concentration influences the sample distribution. The diffusion constant equation for a spherical object is

$$\frac{\bar{x}^2}{t} = D = \frac{k_B T}{6\pi\eta r}$$

where $\bar{x}$ is the moving distant, assuming to 200nm, the maximum thickness of cryoEM sample, k_B is Boltzmann's constant, T is room temperature in this case (300K), η as viscosity ($1\ mPa \cdot S$), and r is the radius for the spherical object. The diffusion finishes within 1.3 mS for a 1.2 MDa protein complex whose average radius is 7nm. A larger particle has larger r, related to a longer time. The diffusion of rotavirus with 35 radius takes 6.4ms. The calculation match with previous estimations of the time scale, in the tens of milliseconds [1]. Diffusion can finish with the time between blotting and plugging if particles are not in their energetically favored status. However, for the particles that have stayed on the air-water interface already, they will not follow the free diffusion model, which explained the uneven distribution.

Chapter 5 Conclusion

In this thesis, the surface domain problem of cryoEM sample was discussed. The theoretical principle was calculated to explain the reason for the air-water interface absorption problem for the cryoEM sample, which induces to heterogeneities and non-physiological states. It obstructed the single particle analysis and high-resolution results. GroEL was a protein with serious air-water interface domain problems and preferred orientation problems. GroEL with different concentrations demonstrated the sample distribution. Surfactant application was proved to be useful in alternating sample distribution. However, it does not have a significant change in the

sample orientation problem. Appropriate concentration fluorinated fos-choline 8 can make fewer particles stay in the air-water interface and did not introduce distinct sample aggregation.

Since the limitation of data quality and quantity, we did not perform the 2D classification to check the improvement of heterogeneity. To better exam the physiological state changing, more images need to be collected to solve the high-resolution density map and compare it with the existing map. 3D reconstruction can provide more information about preferred orientation by comparing the incomplete part of the 3D Fourier space.

For now, the surfactant is applied before blotting, which might affect the blotting process, including but not only blotting time and blotting force. To remove variances, the surfactant applied after blotting is a new direction. The ideal surfactant should be evenly applied to the grid within the short time between blotting and plugging. Gaseous surfactant is a right candidate which can be introduced to the buffer evenly by evaporation after blotting (Figure 6.1). *n-amyl* and *n-decyl alcohol* [41] are potential candidates due to the volatility of fatty alcohols. They will stay on the air-water interface to prevent the adsorption from samples. Industrial gaseous surfactants like *3,5-Dimethyl-1-hexyn-3-ol* will not be considered here because they are toxic.

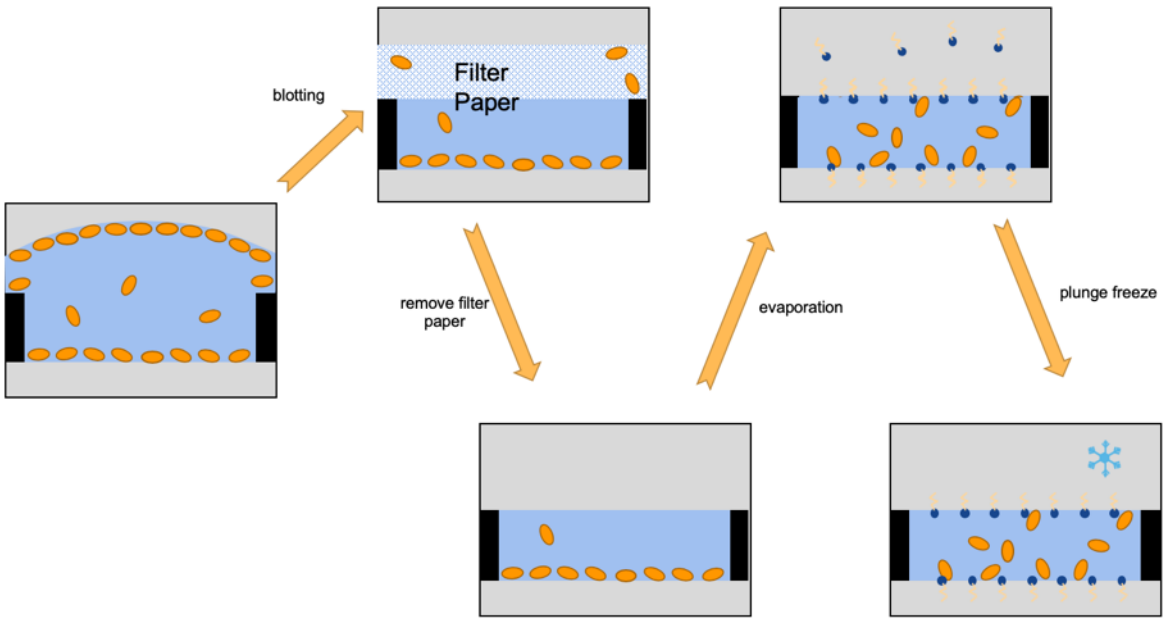

Figure 6.1 Schematic diagram for gaseous surfactant applications.

All experiments are done on GroEL, which is stable, and the structure information is well known. It is a good test sample. Nevertheless, different protein has different properties which have an influence on sample interaction and destruction. Some samples are unstable and easy to aggregation during the sample preparation step. After a guideline about surfactant type and concentration work on GroEL, other real samples will be tested using our guideline to confirm it further.

References:

[1] A.J. Noble, V.P. Dandey, H. Wei, J. Brasch, J. Chase, P. Acharya, Y.Z. Tan, Z. Zhang, L.Y. Kim, G. Scapin, M. Rapp, E.T. Eng, W.J. Rice, A. Cheng, C.J. Negro, L. Shapiro, P.D. Kwong, D. Jeruzalmi, A. des Georges, C.S. Potter, B. Carragher, Routine single particle cryoEM sample and grid characterization by tomography, eLife, 7 (2018) e34257.

[2] J. Dubochet, E. Knapek, Ups and downs in early electron cryo-microscopy, PLoS Biol, 16 (2018) e2005550-e2005550.

[3] Z.H. Zhou, Towards atomic resolution structural determination by single-particle cryo-electron microscopy, Curr Opin Struct Biol, 18 (2008) 218-228.

[4] L. Gan, G.J. Jensen, Electron tomography of cells, Quarterly Reviews of Biophysics, 45 (2012) 27-56.

[5] M. Van Heel, Angular reconstitution: A posteriori assignment of projection directions for 3D reconstruction, Ultramicroscopy, 21 (1987) 111-123.

[6] P.A. Penczek, R.A. Grassucci, J. Frank, The ribosome at improved resolution: New techniques for merging and orientation refinement in 3D cryo-electron microscopy of biological particles, Ultramicroscopy, 53 (1994) 251-270.

[7] V. Lučič, A. Rigort, W. Baumeister, cryo-electron tomography: the challenge of doing structural biology in situ, J Cell Biol, 202 (2013) 407-419.

[8] A. Al-Amoudi, J.-J. Chang, A. Leforestier, A. McDowall, L.M. Salamin, L.P.O. Norlén, K. Richter, N.S. Blanc, D. Studer, J. Dubochet, cryo-electron microscopy of vitreous sections, EMBO J, 23 (2004) 3583-3588.

[9] E. Villa, M. Schaffer, J.M. Plitzko, W. Baumeister, Opening windows into the cell: focused-ion-beam milling for cryo-electron tomography, Curr Opin Struct Biol, 23 (2013) 771-777.

[10] J.R. Kremer, D.N. Mastronarde, J.R. McIntosh, Computer Visualization of Three-Dimensional Image Data Using IMOD, Journal of Structural Biology, 116 (1996) 71-76.

[11] D.M. Bappy, I. Jeon, Modified simultaneous iterative reconstruction technique for fast, high-quality CT reconstruction, IET Image Processing, 11 (2017) 701-708.

[12] W. Wan, J.A.G. Briggs, Chapter Thirteen - cryo-Electron Tomography and Subtomogram Averaging, in: R.A. Crowther (Ed.) Methods in Enzymology, Academic Press2016, pp. 329-367.

[13] D. Lyumkis, Challenges and opportunities in cryo-EM single-particle analysis, J Biol Chem, 294 (2019) 5181-5197.

[14] Y.F. Yano, E. Arakawa, W. Voegeli, C. Kamezawa, T. Matsushita, Initial Conformation of Adsorbed Proteins at an Air–Water Interface, The Journal of Physical Chemistry B, 122 (2018) 4662-4666.

[15] M. Singh-Zocchi, J. Hanne, G. Zocchi, Plastic Deformation of Protein Monolayers, Biophysical Journal, 83 (2002) 2211-2218.

[16] B. Kalinowska, M. Banach, Z. Wiśniowski, L. Konieczny, I. Roterman, Is the hydrophobic core a universal structural element in proteins?, J Mol Model, 23 (2017) 205-205.

[17] E. D'Imprima, D. Floris, M. Joppe, R. Sánchez, M. Grininger, W. Kühlbrandt, Protein denaturation at the air-water interface and how to prevent it, eLife, 8 (2019) e42747.

[18] R.M. Glaeser, How good can cryo-EM become?, Nature Methods, 13 (2016) 28-32.

[19] R.M. Glaeser, B.-G. Han, Opinion: hazards faced by macromolecules when confined to thin aqueous films, Biophysics Reports, 3 (2017) 1-7.

[20] Y.Z. Tan, P.R. Baldwin, J.H. Davis, J.R. Williamson, C.S. Potter, B. Carragher, D. Lyumkis, Addressing preferred specimen orientation in single-particle cryo-EM through tilting, Nature methods, 14 (2017) 793-796.

[21] Y.F. Yano, E. Arakawa, W. Voegeli, T. Matsushita, Real-time investigation of protein unfolding at an air-water interface at the 1 s time scale, J Synchrotron Radiat, 20 (2013) 980-983.

[22] H.H.J. de Jongh, H.A. Kosters, E. Kudryashova, M.B.J. Meinders, D. Trofimova, P.A. Wierenga, Protein adsorption at air–water interfaces: A combination of details, Biopolymers, 74 (2004) 131-135.

[23] S.-H. Roh, C.F. Hryc, H.-H. Jeong, X. Fei, J. Jakana, G.H. Lorimer, W. Chiu, Subunit conformational variation within individual GroEL oligomers resolved by cryo-EM, Proceedings of the National Academy of Sciences, 114 (2017) 8259-8264.

[24] A. Bartesaghi, A. Merk, S. Banerjee, D. Matthies, X. Wu, J.L.S. Milne, S. Subramaniam, 2.2 Å resolution cryo-EM structure of β-galactosidase in complex with a cell-permeant inhibitor, Science, 348 (2015) 1147-1151.

[25] M. Khoshouei, M. Radjainia, W. Baumeister, R. Danev, cryo-EM structure of haemoglobin at 3.2 Å determined with the Volta phase plate, Nat Commun, 8 (2017) 16099-16099.

[26] J. Zeilstra-Ryalls, O. Fayet, C. Georgopoulos, THE UNIVERSALLY CONSERVED GroE (Hsp60) CHAPERONINS, Annual Review of Microbiology, 45 (1991) 301-325.

[27] V.V. Marchenkov, G.V. Semisotnov, GroEL-assisted protein folding: does it occur within the chaperonin inner cavity?, Int J Mol Sci, 10 (2009) 2066-2083.

[28] I. Drulyte, R.M. Johnson, E.L. Hesketh, D.L. Hurdiss, C.A. Scarff, S.A. Porav, N.A. Ranson, S.P. Muench, R.F. Thompson, Approaches to altering particle distributions in cryo-electron microscopy sample preparation, Acta Crystallogr D Struct Biol, 74 (2018) 560-571.

[29] R.M. Glaeser, PROTEINS, INTERFACES, AND CRYO-EM GRIDS, Curr Opin Colloid Interface Sci, 34 (2018) 1-8.

[30] Z.L. Johnson, J. Chen, Structural Basis of Substrate Recognition by the Multidrug Resistance Protein MRP1, Cell, 168 (2017) 1075-1085.e1079.

[31] T.E.T. Hughes, D.T. Lodowski, K.W. Huynh, A. Yazici, J. Del Rosario, A. Kapoor, S. Basak, A. Samanta, X. Han, S. Chakrapani, Z.H. Zhou, M. Filizola, T. Rohacs, S. Han, V.Y. Moiseenkova-Bell, Structural basis of TRPV5 channel inhibition by econazole revealed by cryo-EM, Nat Struct Mol Biol, 25 (2018) 53-60.

[32] S. Basak, Y. Gicheru, S. Rao, M.S.P. Sansom, S. Chakrapani, cryo-EM reveals two distinct serotonin-bound conformations of full-length 5-HT(3A) receptor, Nature, 563 (2018) 270-274.

[33] N.M. Kovalchuk, A. Trybala, V. Starov, O. Matar, N. Ivanova, Fluoro- vs hydrocarbon surfactants: Why do they differ in wetting performance?, Advances in Colloid and Interface Science, 210 (2014) 65-71.

[34] K.-H. Park, C. Berrier, F. Lebaupain, B. Pucci, J.-L. Popot, A. Ghazi, F. Zito, Fluorinated and hemifluorinated surfactants as alternatives to detergents for membrane protein cell-free synthesis, Biochem J, 403 (2007) 183-187.

[35] C.M. Oikonomou, M.T. Swulius, A. Briegel, M. Beeby, Q. Yao, Y.W. Chang, G.J. Jensen, Chapter 4 - Electron cryotomography, in: C. Harwood, G.J. Jensen (Eds.) Methods in Microbiology, Academic Press2016, pp. 115-139.

[36] Y. Liu, D.T. Huynh, T.O. Yeates, A 3.8 Å resolution cryo-EM structure of a small protein bound to an imaging scaffold, Nat Commun, 10 (2019) 1864-1864.

[37] Q. Fang, D. Zhu, I. Agarkova, J. Adhikari, T. Klose, Y. Liu, Z. Chen, Y. Sun, M.L. Gross, J.L. Van Etten, X. Zhang, M.G. Rossmann, Near-atomic structure of a giant virus, Nat Commun, 10 (2019) 388-388.

[38] C.-H. Chu, I. Sarangadharan, A. Regmi, Y.-W. Chen, C.-P. Hsu, W.-H. Chang, G.-Y. Lee, J.-I. Chyi, C.-C. Chen, S.-C. Shiesh, G.-B. Lee, Y.-L. Wang, Beyond the Debye length in high ionic strength solution: direct protein detection with field-effect transistors (FETs) in human serum, Sci Rep, 7 (2017) 5256-5256.

[39] Robert M. Glaeser, B.-G. Han, R. Csencsits, A. Killilea, A. Pulk, Jamie H.D. Cate, Factors that Influence the Formation and Stability of Thin, cryo-EM Specimens, Biophysical Journal, 110 (2016) 749-755.

[40] E.Y. Gatapova, I.A. Graur, O.A. Kabov, V.M. Aniskin, M.A. Filipenko, F. Sharipov, L. Tadrist, The temperature jump at water – air interface during evaporation, International Journal of Heat and Mass Transfer, 104 (2017) 800-812.

[41] K. Małysa, K. Khristov, D. Exerowa, Surfactant in the gaseous phase I. Formation of foams and thin liquid films, Colloid and Polymer Science, 269 (1991) 1045-1054.